

CHARACTERIZING INTRA-CLUSTER LIGHT AT  $z \sim 0.5$  IN THE HUBBLE FRONTIER FIELDSTAKAHIRO MORISHITA<sup>1,2,3</sup>, LOUIS E. ABRAMSON<sup>1</sup>, TOMMASO TREU<sup>1</sup>, KASPER B. SCHMIDT<sup>4</sup>, BENEDETTA VULCANI<sup>5</sup>, XIN WANG<sup>1</sup>*Submitted to The Astrophysical Journal Letters*

## ABSTRACT

We investigate the intra-cluster light (ICL) in 4 Hubble Frontier Fields clusters at  $0.3 < z < 0.6$ . Our new method makes use of the unprecedented depth of *Hubble Space Telescope* imaging data to probe very diffuse light ( $\mu_{F160W} \sim 29.5$  mag arcsec<sup>-2</sup>) out to clustro-centric radii  $R_{cl} \sim 300$  kpc. The rest-frame  $B-V$  color of the ICL is consistent with that of passive cluster galaxies of  $\log M_*/M_\odot < 9.5$ ,  $\sim 0.3$  mag bluer than more massive ones ( $\log M_*/M_\odot > 10.5$ ) and the cores of the brightest cluster galaxies, implying that the ICL and more-massive cluster galaxies are built-up via distinct processes. The stellar mass of the ICL ranges from  $11.1 < \log M_*^{ICL}/M_\odot < 11.9$ , implying an ICL stellar mass fraction of  $\sim 10$ -20%, about half of the local value. Hence, we posit that the amount of ICL has rapidly increased since  $z \sim 1$ , and *is still being constructed*, at a rate of  $\sim 200 M_\odot \text{ yr}^{-1}$  at  $z \sim 0.5$  by cluster specific mechanisms such as galaxy interactions and the stripping of low-mass galaxies.

**Keywords:** galaxies: evolution — galaxies: cluster — galaxies: ICL

## 1. INTRODUCTION

Intra-cluster light (ICL) is starlight that fills the intergalactic space in dense galaxy environments. First proposed by Zwicky (1937), it is unique to galaxy groups and clusters, suggesting that its formation process is related to environment-specific phenomena that may also influence galaxies. Thus, understanding the origin and evolution of the ICL may aid our understanding of galaxy evolution.

Numerical calculations suggest that the ICL in massive clusters ( $\log M_{500}/M_\odot \sim 15$ ) formed at  $z < 1$ , epochs when massive cluster galaxies (including brightest cluster galaxies; BCGs) had nearly completed their stellar mass accumulation (Murante et al. 2007; Collins et al. 2009; Contini et al. 2014; Burke et al. 2015). Some fractions of stars in cluster member galaxies remain in clusters after cluster specific mechanisms, such as stellar/gas stripping and interaction between galaxies and dark matter (Larson et al. 1980; Nipoti et al. 2003; McPartland et al. 2016). However, observational constraints on, e.g., its origin and formation rate, have been limited largely due to the low surface brightness of the ICL (e.g., Zaritsky et al. 2004; Gonzalez et al. 2007; Guennou et al. 2012; Pre-sotto et al. 2014, but see also Zibetti et al. 2005 who stack 683 SDSS clusters at  $0.2 < z < 0.3$ ), and difficulties introduced by the fact that other cluster galaxies are, by definition, embedded within it.

In this letter, we utilize deep *Hubble Space Telescope* (HST) multi-band imaging from *Hubble Frontier Fields* (HFF; Lotz et al. 2016) to overcome these obstacles, dissecting the ICL in four clusters at  $z \sim 0.5$ —when it is being rapidly assembled—out to  $R_{cl} \sim 300$  kpc. We develop a new method to extract the ICL without any assumption on its light

profile, relying only on much more robust knowledge of individual *galaxy* light profiles. By combining the deep data and our new method, we can infer the ICL’s:

1. rest-frame colors, and therefore its stellar population and age;
2. total stellar mass, and therefore formation timescale, by using comparisons with local clusters.

As we have a complete galaxy census ( $\log M_*/M_\odot \sim 7.8$ ) of each of these clusters (Morishita et al. 2016, hereafter M16), we can also attempt to quantitatively link the ICL to its probable cluster galaxy progenitors/sources.

Below,  $\Omega_m = 0.3$ ,  $\Omega_\Lambda = 0.7$  and  $H_0 = 70 \text{ km s}^{-1} \text{ Mpc}^{-1}$ , and we assume a Chabrier (2003) initial mass function when estimating stellar masses. All magnitudes are quoted in the AB system (Oke & Gunn 1983; Fukugita et al. 1996).

## 2. DATA AND METHOD

We base our analysis on the first four HFF clusters with complete data: Abell2744, MACS0416, MACS0717, and MACS1149. The HFF imaging spans ACS F435/606/814W through WFC3IR F105/125/140/160W filters. The limiting surface brightness ( $S/N > 3$  per pixel) is  $\mu_{F160W} \sim 29.5$  mag arcsec<sup>-2</sup>.

All ICL measurements are derived from the HFF cluster central (CLS) pointing. The HFF parallel (PR1) pointings lie at  $R_{cl} \gtrsim 2$  Mpc and therefore contain negligible ICL. We use these data to estimate our background uncertainties (Section 2.1).

The method is schematically shown in Figure 1. We first detect all the sources on the composite image using SExtractor (Bertin & Arnouts 1996). For galaxies with  $m_{F160W} < 26$  ( $\sim 400$ -900 in each cluster), where structural fitting is reliable, we fit single Sérsic light profiles using GALFIT (Peng et al. 2002) in  $300 \times 300$  pixel postage stamp (see M16).

At the same time, we fit the local sky background as a constant for each postage stamp. The estimated sky is dominated by the ICL, but has also some contribution from non-ICL component (e.g., zodiacal light). Although this is small in

mtaka@astro.ucla.edu

<sup>1</sup> Department of Physics and Astronomy, University of California, Los Angeles, CA 90095-1547, USA<sup>2</sup> Astronomical Institute, Tohoku University, Aramaki, Aoba, Sendai 980-8578, Japan<sup>3</sup> Institute for International Advanced Research and Education, Tohoku University, Aramaki, Aoba, Sendai 980-8578, Japan<sup>4</sup> Leibniz-Institut für Astrophysik Potsdam (AIP), An der Sternwarte 16, D-14482 Potsdam, Germany<sup>5</sup> School of Physics, The University of Melbourne, VIC 3010, Australia

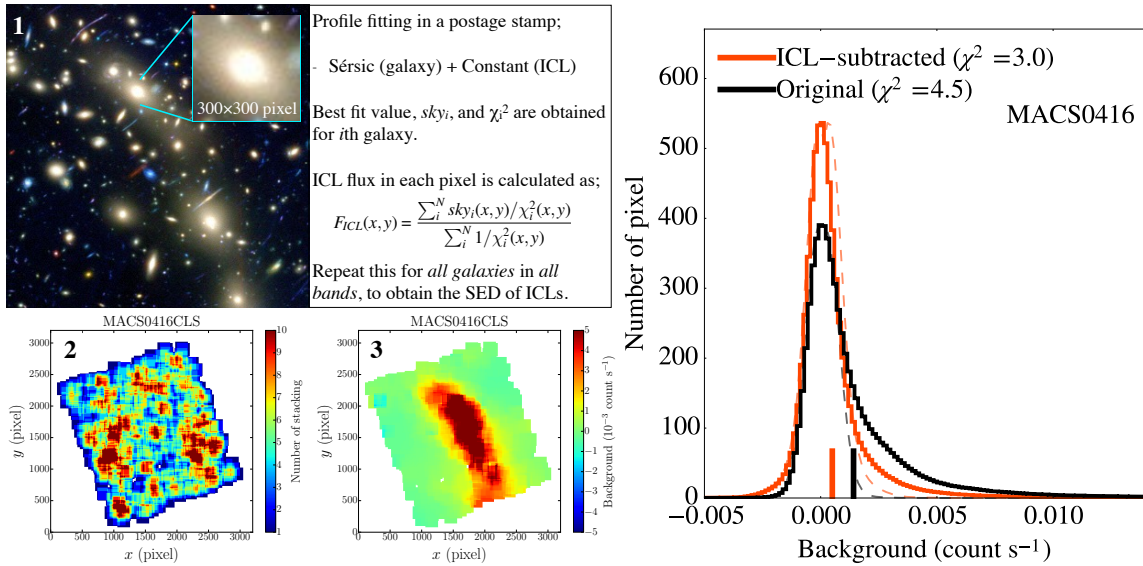


**Figure 1.** *Left:* Schematic view of ICL-subtraction method: 1. We fit the galaxy light profile and local sky background for each target galaxies in M16, and 2. stack the modeled sky in overlapped pixels and stack over the FoV of WFC3 ( $\sim 300$  kpc) to construct the ICL map. 3. The stacking is weighted by the inverse of  $\chi^2$  values of the light profile fitting (Eq. 1). *Right:* Comparison of two histograms for the pixel values in ICL-subtracted (red line) and original (black) images. An asymmetric distribution (excess of positive pixel, i.e. ICL) is observed in the original one, while the distribution is more symmetric for the ICL-subtracted image, as the medians of distributions indicate (bars of same colors as the distributions). The fit with a symmetric function for each distribution (dashed lines) and its goodness ( $\chi^2$ ) are shown.

the IR bands, this is not true at bluer wavelengths where the ICL is faint (see below).

After estimating the galaxy light profiles and local sky backgrounds for all the detected sources, we then reconstruct the ICL by stacking the modeled sky images. Since some postage stamps overlap, we calculate the representative value in each pixel,  $F_{ICL}(x, y)$ , by taking the weighted mean as

$$F_{ICL}(x, y) = \frac{\sum_i^N sky_i(x, y) / \chi_i^2(x, y)}{\sum_i^N 1 / \chi_i^2(x, y)}, \quad (1)$$

where  $sky_i(x, y)$  is the best fit sky background in a given pixel and  $\chi_i^2(x, y)$  is from GALFIT for the  $i$ -th galaxy. We repeat this analysis for all bands before fitting ICL SEDs (Section 2.2).

Although we have pixel-by-pixel information, we focus on integrated ICL properties below. This is because systematic uncertainties (Section 2.1) are non-negligible and will need to be appropriately treated before, e.g., radial trends can be properly examined using the HFF or similar data (e.g., Presotto et al. 2014; Montes & Trujillo 2014; DeMaio et al. 2015).

Figure 1 shows the histogram of pixel background values in one of our clusters (MACS0416). Background pixels are those without galaxy source light as defined using the SExtractor segmentation map. The comparison between the original and ICL-subtracted images clearly shows that the former has an asymmetric tail to positive values while the latter is more symmetric about zero. Fit with a symmetric function probes this ( $\chi^2 = 4.5$  and  $3.0$ , respectively). We note that the negative tail of ICL-subtracted image is similar to the original image’s—ICL over-subtraction would lead to a negative excess, which is not seen. This suggests that our ICL subtraction (equivalently, ICL image construction; Figure 2) is robust.

### 2.1. Uncertainties in the ICL Maps

Statistical uncertainties—estimated from RMS maps made publicly available by the HFF team—are very small given the large numbers of pixels we are summing over.

In contrast, systematic uncertainties—dominated by larger-scale background fluctuations caused, e.g., by zodiacal light and earth glow (Brammer et al. 2014)—are significant. Though they are partially suppressed by the *HST* reduction pipeline,<sup>6,7</sup> the residuals are sizable relative to the intrinsically faint signal from the ICL.

The effects of these residuals are estimated using the PR1 data, where the ICL contribution is negligible. We apply the same method to the PR1 field to reconstruct an (ICL-free) background map, and see the variance from the mean values as a function of bandpass. We adopt these values as our ICL flux errors in the SED fitting procedure. They amount to  $\sim 30\%$  in F160W and  $\sim 50\%$  in F606W.<sup>8</sup> We ignore the comparatively small statistical errors below.

### 2.2. Physical Parameter Estimates

The ICL’s stellar mass and rest-frame colors are derived using FAST (Kriek et al. 2009). The input photometry is conducted on a common, resampled pixel grid for all filters. Pixels either on or near bright stars are masked. The systematic errors estimated in Section 2.1 are used in the SED fitting. Table 1 summarizes the results.

For consistency with the galaxy properties derived by M16, we assume a Chabrier IMF and exponential star formation history for the ICL. The only difference here is our choice of a

<sup>6</sup> <http://www.stsci.edu/hst/campaigns/frontier-fields/FF-Data>

<sup>7</sup> <https://blogs.stsci.edu/newsletter/files/2015/03/FFCalibration.pdf>

<sup>8</sup> F435W is dominated by the error, so we only quote upper-limits in that band. Note that changing the size of the fitting postage stamps (from, e.g., 300 to 200 pixel) results in  $< 10\%$  increases in F160W, which is much smaller than the background uncertainty.

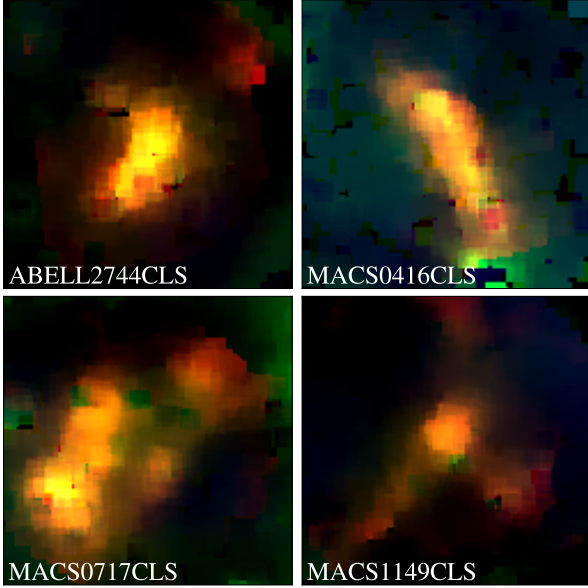


**Figure 2.** RGB image of 4 ICL maps (blue:F435W, green:F125W, red:F160W). The image size, 2900×2900 pixel, is comparable to the FoV of WFC3.

dust-free SED model for the ICL and BCGs. This assumption is reasonable for our purposes: there is no indication that the ICL nor BCGs is very dusty (e.g., Kitayama et al. 2009).

Some studies report radial ICL metallicity gradients (e.g., Montes & Trujillo 2014), but because we work with spatially integrated (i.e., light-weighted) ICL data, we fixed this quantity uniformly to a super-solar value ( $Z = 2.5Z_{\odot}$ , where  $Z_{\odot} = 0.02$  is the solar metallicity). SED fitting results of ICL and BCGs prefer super-solar to solar or sub-solar ( $Z = 0.4Z_{\odot}$ ) metallicities: the bright metal-rich central ICL regions dominate over the faint less metal rich outskirts (e.g., DeMaio et al. 2015, see also Figure 3). Regardless, the effect of changing the assumed metallicity from super-solar to solar causes its stellar mass to increase only by  $\sim 10\%$ , which does not alter our conclusions.

All quantities are derived similarly for the cluster BCGs for comparison. Two BCGs are selected in each cluster by visual inspection. The location and number of the BCGs agree with lens models<sup>9</sup> in most of clusters. BCGs are known to have diffuse envelopes extending to  $R > 100$  kpc, and the stellar mass estimated by SExtractor measurements (MAG\_AUTO; see M16) is underestimated. We correct for this using the GALFIT Sérsic model magnitude.

### 3. RESULTS

#### 3.1. ICL Colors

Figure 3 shows the rest-frame colors of the ICLs of the four HFF clusters. We use a  $BVJ$  color-color diagram to examine the age and metallicity of the ICLs' stellar populations. This avoids complexities associated with inferring rest-frame  $U$ -band-dependent colors due to the poor  $S/N$  in the F435W maps. The age-metallicity grid is based on a dust-free stellar population model (Bruzual & Charlot 2003) consistent with those used in the ICL/BCG SED fitting.

BCG colors are shown for comparison. These occupy the *right-top* region of the diagram, implying more ma-

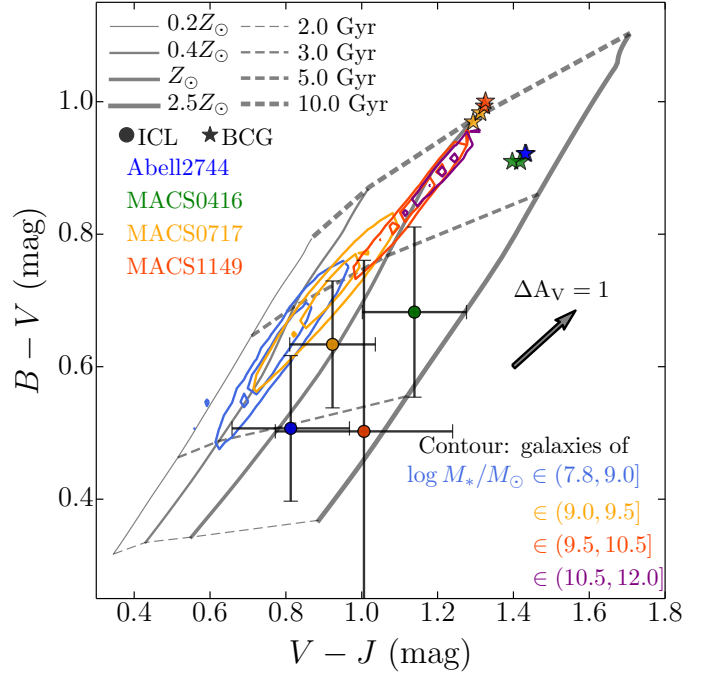


**Figure 3.** Rest-frame colors of ICL (circles) in  $BVJ$  diagram. The dashed and solid lines are grids for metallicity and ages, calculated with Bruzual & Charlot (2003) model. The underlying contours are the colors of cluster galaxies in four stellar mass bins, which are bounded at  $\log M_*/M_{\odot} = 9.0, 9.5$  and  $10.5$ . The ICL colors are consistent with those of  $\log M_*/M_{\odot} < 9.5$  galaxies, while all BCGs reside the redder region (stars). The effect by dust attenuation ( $A_V = 1.0$  mag) on the grids is indicated with an arrow.

ture/older/more metal-rich stellar populations than those in the ICL. That said, the BCGs in this study have color gradients of  $d(B-V)/dR \sim 0.006$  mag kpc<sup>-1</sup>, implying a smooth BCG/ICL transition at  $R \sim 50$  kpc.

Colors of normal cluster galaxies are taken from M16 and shown in the background contours, grouped into three stellar mass bins near  $\log M_*/M_{\odot} = 9.0, 9.5$ , and  $10.5$ . Since quiescent galaxies dominate in cluster cores, the blue cluster population is not clearly seen within the presented contour range (see also M16 Figures 3 and 4). We see the consistency of ICL and  $\log M_*/M_{\odot} < 9.5$  galaxies colors within errors.

Hence, taken at face value, Figure 3 implies that whatever process built the ICL was distinct from that which built BCGs, but may be related to the formation of comparatively low-mass ( $\log M_*/M_{\odot} < 9.5$ ) cluster galaxies. We return to this point in Section 4.

#### 3.2. ICL Mass Fractions

The ICL mass fraction in clusters is an physically interesting quantity because it is a metric of how ICL formation proceeds with respect to cluster galaxy evolution. Figure 4 (and Table 1) summarizes the total masses of the ICL component ( $M_{*}^{\text{ICL}}$ ) and ICL+galaxies ( $M_{*}^{\text{tot}}$ ) in each cluster system. The total stellar mass is calculated in each cluster by summing the masses of cluster galaxies with  $\log M_*/M_{\odot} > 7.8$  (see M16; the contribution from lower-mass systems is negligible).

The stellar mass in ICL ranges in  $11.1 < \log M_{*}^{\text{ICL}}/M_{\odot} < 11.9$ —similar to that of the BCGs. We note that our measurement for Abell 2744 ( $\log M_{*}^{\text{ICL}}/M_{\odot} \sim 11.18$ ) is consistent with previous results derived from the same data used here (Montes & Trujillo 2014).

The median ICL fraction,  $M_{*}^{\text{ICL}}/M_{*}^{\text{tot}}$ , is  $\sim 10$ – $20\%$  (Fig-

<sup>9</sup><https://archive.stsci.edu/prepds/frontier/lensmodels/>



**Table 1**  
Cluster and ICL properties.

Cluster	Redshift	$r_{\text{FoV}}$ (Mpc)	$(B-V)_{\text{ICL}}$ (mag)	$(V-J)_{\text{ICL}}$ (mag)	$M_{\text{ICL}}^*$ ( $10^{11} M_{\odot}$ )	$M_{\text{tot}}^*$ ( $10^{11} M_{\odot}$ )	$M_{500}$ ( $10^{14} M_{\odot}$ )	$M_{500}^{\text{FoV}}$ ( $10^{14} M_{\odot}$ )	$M_{\text{ICL}}^*/M_{\text{tot}}^*$	$\Omega_*/\Omega_{\text{tot}}$
Abell2744	0.308	0.27	$0.51 \pm 0.11$	$0.81 \pm 0.15$	$1.29^{+1.17}_{-0.29}$	$15.12^{+0.21}_{-0.13}$	$17.6 \pm 2.3$	$1.92 \pm 0.25$	$0.08^{+0.08}_{-0.02}$	$0.009 \pm 0.002$
MACS0416	0.396	0.32	$0.68 \pm 0.13$	$1.14 \pm 0.14$	$4.68^{+5.32}_{-1.37}$	$21.80^{+0.11}_{-0.09}$	$9.1 \pm 2.0$	$1.37 \pm 0.30$	$0.22^{+0.25}_{-0.06}$	$0.019 \pm 0.010$
MACS0717	0.548	0.38	$0.63 \pm 0.10$	$0.92 \pm 0.11$	$8.71^{+1.17}_{-1.47}$	$65.00^{+0.13}_{-0.07}$	$24.9 \pm 2.7$	$4.30 \pm 0.47$	$0.13^{+0.06}_{-0.02}$	$0.018 \pm 0.003$
MACS1149	0.544	0.38	$0.50 \pm 0.26$	$1.00 \pm 0.23$	$4.17^{+6.35}_{-1.98}$	$57.35^{+0.09}_{-0.07}$	$18.7 \pm 3.0$	$3.51 \pm 0.56$	$0.08^{+0.12}_{-0.04}$	$0.017 \pm 0.006$

**Note.** — Stellar mass is derived with the Chabrier IMF for galaxies, ICL, and BCGs. Dust extinction is set to be zero and metallicity is the super-solar value ( $Z = 2.5Z_{\odot}$ ) for ICL and BCG.

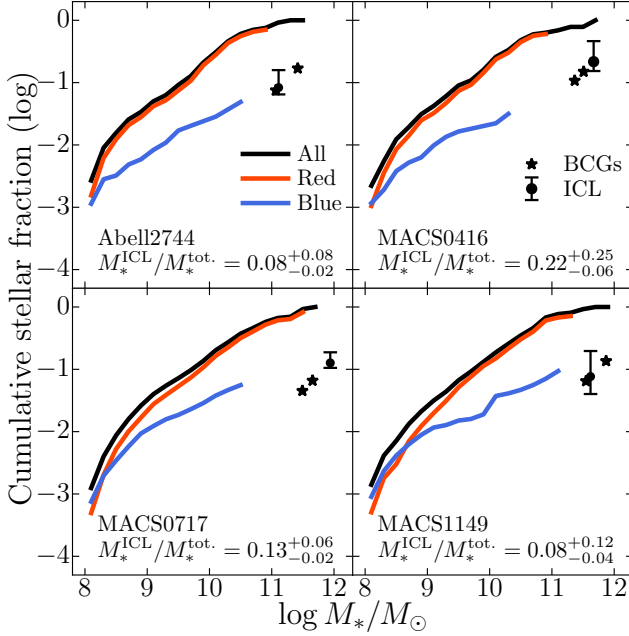


**Figure 4.** Cumulative total stellar masses in 4 clusters. The total stellar mass is the sum of star-forming (blue lines) and quiescent (red lines) cluster galaxies, ICL (circles), and BCGs (stars). The values are normalized to stress the fraction of ICL over the total stellar mass in each system,  $M_{\text{ICL}}^*/M_{\text{tot}}^*$ . The total stellar mass in the star-forming galaxies is deficit for the ICL mass by itself, while passive systems have enough for ICL.

ure 4), which is about half of the local value ( $\sim 40\%$ ; Gonzalez et al. 2013), and consistent with the previous results at similar redshifts (e.g., Burke et al. 2015), and theoretical expectations (e.g., Rudick et al. 2011; Contini et al. 2014). As such, we can state that the ICL will double in mass between  $z \sim 0.5$  and today. This is to be contrasted with the fact that at  $z \sim 0.5$  BCG cores have essentially completed their formation (e.g., Gallazzi et al. 2014), strengthening the distinct formation scenarios inferred from the  $BVJ$  diagram (Figure 3).

We show the cumulative stellar mass fractions in red and blue galaxies in Figure 4. At the clustro-centric radii probed by the CLS pointings, the total stellar mass in star forming cluster galaxies is  $< 10\%$  of that in passive systems and  $\sim 10\text{--}50\%$  of the ICL’s (except in MACS1149, where they are equal). In terms of ICL formation pathways, this would suggest that the ICL may principally arise from the “post-processing” of cluster passive galaxies, as opposed to the pre-processing of infalling blue galaxies (see Section 4).

The estimated total stellar fraction (ICL+BCGs+normal galaxies,  $\Omega_*$ ) over the total mass (baryonic + dark matter,  $\Omega_{\text{tot}}$ ) in the clusters is  $\sim 1.8\%$  except for Abell 2744 of  $0.9\%$ .

Total cluster masses are estimated by correcting the values of  $M_{500}$ —the mass within a radius where the cluster’s density exceeds  $500\times$  the critical density of the universe—from Mantz et al. (2010) for our FoV. The measurements of total stellar fraction, yet through an indirect method, are consistent at  $1\text{--}\sigma$  with a measurement by Wang et al. (2015) and at  $2\text{--}\sigma$  by Hoag et al. (2016). We see no dependence of baryon fractions on halo mass and redshift (cf. Gonzalez et al. 2007, who see an anti-correlation).

#### 4. DISCUSSION

We discuss possible scenarios for the origin and evolution of the ICL based on the color and mass measurements described above and those of  $z \approx 0$  clusters.

Comparing our measurements to those of Gonzalez et al. (2013) and computational predictions (Martel et al. 2012; Contini et al. 2014), ICL mass fractions must approximately double between  $z \sim 0.5$  and today. This implies growth rates of  $\sim 10^{12} M_{\odot}/5 \text{ Gyr} = 200 M_{\odot} \text{ yr}^{-1}$ . This is a relatively high absolute growth rate, but since these clusters harbor hundreds to thousands of galaxies, it can be sustained from relatively small leaks on a per-galaxy basis. The stars giving rise to this mass growth of the ICL potentially comes from newly accreted galaxies, or the “post-processing” of already acquired (likely passive) cluster galaxies.

Under the first scenario, since many of the newly accreted galaxies will have been recently starforming (e.g., Dressler et al. 2013), we might expect the ICL colors to remain relatively blue compared to the general, mature cluster galaxy population. On the other hand, if the ICL was mainly grown by post-processing, there would be no substantive blue population from which to draw ICL stars, so we would expect passive evolution (of the older ICL component and the source galaxies) to redden the observed ICL over time.

Studies of the Virgo cluster—which is less massive and therefore, if anything, younger than the descendants of our clusters—show its ICL to have  $B-V \sim 0.8\text{--}1$  (Castro-Rodríguez et al. 2009; Rudick et al. 2010, see also Zibetti et al. 2005 for SDSS clusters at  $0.2 < z < 0.3$ ), about  $0.2$  mag redder than what we observe, though in consistent for some of our clusters within error. Our calculation based on a stellar population model (Galaxev; Bruzual & Charlot 2003) shows the passive evolution of the observed population would be consistent with the Virgo color. Hence, it would appear that, at least at *later* times ( $z \lesssim 0.5$ ), ICL growth is driven substantially by the removal of stars from the established cluster population rather than infalling (at least recently starforming) systems.

The origin of the ICL already established in the HFF sample is hazier. Regardless of the source of the stars, our findings suggest that the  $z \sim 0.5$  ICL is dominated by those with

ages  $\sim 3\text{--}4$  Gyr, implying its construction began at redshifts of  $z \lesssim 1.4$ . This qualitatively concurs with Montes & Trujillo (2014)’s observations of Abell2744, and numerical predictions by Contini et al. (2014).

Also in agreement with Montes & Trujillo (2014), the *BVJ* diagram shows that the ICL’s rest-frame colors to be more consistent with those of  $\log M_*/M_\odot < 9.5$  galaxies than they are with those of (at least the cores of) more massive galaxies or BCGs, which are  $\sim 0.3$  mag redder in  $B-V$  and therefore presumably much older. Given that lower-mass cluster galaxies are also much more abundant than their higher-mass counterparts (e.g., M16), this finding would argue for the ICL to come more from the stripping/cannibalism (e.g., Ostriker & Tremaine 1975; Moore et al. 1996; Treu et al. 2003; Nipoti et al. 2003, 2004) of low-mass ( $\log M_*/M_\odot \lesssim 10$ ), as opposed to even Milky Way mass galaxies. Given the results of M16 (see their Figures 9 and 11), perhaps half of these were already in the cluster at  $z \sim 1$ , with the remainder having been accreted subsequently, and so could indeed serve as a substantial ICL source population.

The interpretation is in opposition to that of Montes & Trujillo (2014) and predictions of Contini et al. (2014), which suggest that Milky Way mass ( $\log M_*/M_\odot \gtrsim 10.5$ ) progenitors are the most likely source for the ICL based on dynamical friction arguments. The presence of strong color gradients in such galaxies could remedy this discrepancy, since the ICL is likely to come from easily stripped stars at large galactocentric radii, which would also be the bluest (Figure 9 in Morishita et al. 2015). Additionally, the ICL mass in our clusters is roughly equal to that of all *extant*  $\log M_*/M_\odot < 10$  red galaxies (Figure 4), implying that some help from higher-mass systems is likely (as favored by Montes & Trujillo 2014). This being said, it seems secure to posit from the HFF data that the ICL does not arise through the same mechanisms that establish at least the high-mass “native” cluster galaxy population, including the BCG core. For example, dynamical friction and the more massive galaxies can be responsible for the ICL very close to BCGs, while the lower mass galaxies and bluer ones are responsible for the rest of the ICL.

Hence, the ICL appears to have arisen at relatively late times with early growth driven by a mix of the stripping of preprocessed galaxies of  $\log M_*/M_\odot \lesssim 10.5$  and the extant cluster population, and later growth (at  $z \lesssim 0.5$ ) being dominated by the latter process (given the red ICL colors of  $z \sim 0$  clusters). Extremely deep imaging of  $z \gtrsim 1$  proto-clusters by JWST and WFIRST will provide crucial leverage on the details of this history.

### 5. SUMMARY

1. We derived the SED properties (stellar mass and rest-frame colors) of ICL by using a new method, which is consistent with the galaxies light profile fitting results.
2. Very deep imaging data allowed us to access the faint stellar component out to  $\sim 300$  kpc from the cluster centers,  $\sim 29.5$  mag arcsec $^{-1}$ , and gave us more accurate measurements of ICL for 4 HFF clusters at  $0.3 < z < 0.6$ .
3. By comparing with BCGs and normal cluster galaxies, we discussed the origin of ICL in terms of colors (i.e. age) and total amount of the stellar mass. The ICL is likely to rapidly form from quiescent cluster galaxies of  $\log M_*/M_\odot < 9.5$  disrupted by stellar stripping since  $z \sim 1.4$ .

4. The stellar mass of the ICL is  $\sim 10\%\text{--}20\%$  of that in galaxies, about a half of the local value, suggesting that the ICL is still under construction at the redshift observed. This also suggests that the ICL needs to be constructed rapidly ( $\sim 200 M_\odot \text{ yr}^{-1}$ ) from  $z \sim 0.5$  to the present date, emphasizing the importance of the cluster-specific mechanism on low-mass galaxies.

Support for this work is provided by NASA through HST-GO-13459. T.M. acknowledges support from the Japan Society for the Promotion of Science (JSPS) through JSPS research fellowships for Young Scientists.

### REFERENCES

- Bertin, E., & Arnouts, S. 1996, *A&AS*, 117, 393
- Brammer, G., Pirzkal, N., McCullough, P., & MacKenty, J. 2014, Time-varying Excess Earth-glow Backgrounds in the WFC3/IR Channel, Tech. rep.
- Bruzual, G., & Charlot, S. 2003, *MNRAS*, 344, 1000
- Burke, C., Hilton, M., & Collins, C. 2015, *MNRAS*, 449, 2353
- Castro-Rodríguez, N., Arnaboldi, M., Aguerri, J. A. L., et al. 2009, *A&A*, 507, 621
- Chabrier, G. 2003, *PASP*, 115, 763
- Collins, C. A., Stott, J. P., Hilton, M., et al. 2009, *Nature*, 458, 603
- Contini, E., De Lucia, G., Villalobos, Á., & Borgani, S. 2014, *MNRAS*, 437, 3787
- DeMaio, T., Gonzalez, A. H., Zabludoff, A., Zaritsky, D., & Bradač, M. 2015, *MNRAS*, 448, 1162
- Dressler, A., Oemler, Jr., A., Poggianti, B. M., et al. 2013, *ApJ*, 770, 62
- Fukugita, M., Ichikawa, T., Gunn, J. E., et al. 1996, *AJ*, 111, 1748
- Gallazzi, A., Bell, E. F., Zibetti, S., Brinchmann, J., & Kelson, D. D. 2014, *ApJ*, 788, 72
- Gonzalez, A. H., Sivanandam, S., Zabludoff, A. I., & Zaritsky, D. 2013, *ApJ*, 778, 14
- Gonzalez, A. H., Zaritsky, D., & Zabludoff, A. I. 2007, *ApJ*, 666, 147
- Guenou, L., Adami, C., Da Rocha, C., et al. 2012, *A&A*, 537, A64
- Hoag, A., Huang, K.-H., Treu, T., et al. 2016, *ArXiv e-prints*, arXiv:1603.00505
- Kitayama, T., Ito, Y., Okada, Y., et al. 2009, *ApJ*, 695, 1191
- Kriek, M., van Dokkum, P. G., Labbé, I., et al. 2009, *ApJ*, 700, 221
- Larson, R. B., Tinsley, B. M., & Caldwell, C. N. 1980, *ApJ*, 237, 692
- Lotz, J. M., Koekemoer, A., Coe, D., et al. 2016, *ArXiv e-prints*, arXiv:1605.06567
- Mantz, A., Allen, S. W., Ebeling, H., Rapetti, D., & Drlica-Wagner, A. 2010, *MNRAS*, 406, 1773
- Martel, H., Barai, P., & Brito, W. 2012, *ApJ*, 757, 48
- McPartland, C., Ebeling, H., Roediger, E., & Blumenthal, K. 2016, *MNRAS*, 455, 2994
- Montes, M., & Trujillo, I. 2014, *ApJ*, 794, 137
- Moore, B., Katz, N., Lake, G., Dressler, A., & Oemler, A. 1996, *Nature*, 379, 613
- Morishita, T., Ichikawa, T., Noguchi, M., et al. 2015, *ApJ*, 805, 34
- Morishita, T., Abramson, L. E., Treu, T., et al. 2016, *ArXiv e-prints*, arXiv:1607.00384
- Murante, G., Giovalli, M., Gerhard, O., et al. 2007, *MNRAS*, 377, 2
- Nipoti, C., Stiavelli, M., Ciotti, L., Treu, T., & Rosati, P. 2003, *MNRAS*, 344, 748
- Nipoti, C., Treu, T., Ciotti, L., & Stiavelli, M. 2004, *MNRAS*, 355, 1119
- Oke, J. B., & Gunn, J. E. 1983, *ApJ*, 266, 713
- Ostriker, J. P., & Tremaine, S. D. 1975, *ApJ*, 202, L113
- Peng, C. Y., Ho, L. C., Impey, C. D., & Rix, H.-W. 2002, *AJ*, 124, 266
- Presotto, V., Girardi, M., Nonino, M., et al. 2014, *A&A*, 565, A126
- Rudick, C. S., Mihos, J. C., Harding, P., et al. 2010, *ApJ*, 720, 569
- Rudick, C. S., Mihos, J. C., & McBride, C. K. 2011, *ApJ*, 732, 48
- Treu, T., Ellis, R. S., Kneib, J.-P., et al. 2003, *ApJ*, 591, 53
- Wang, X., Hoag, A., Huang, K.-H., et al. 2015, *ApJ*, 811, 29
- Zaritsky, D., Gonzalez, A. H., & Zabludoff, A. I. 2004, *ApJ*, 613, L93
- Zibetti, S., White, S. D. M., Schneider, D. P., & Brinkmann, J. 2005, *MNRAS*, 358, 949
- Zwicky, F. 1937, *ApJ*, 86, 217